Title

CREEP AND DENSIFICATION DURING SINTERING OF GLASS POWDER COMPACTS: II. EFFECTS OF PARTICLE SIZE

Authors

Rahaman, M.N.
Jonghe, L.C. De
Brook, R.J.

Publication Date

1985-12-01

Lawrence Berkeley Laboratory
UNIVERSITY OF CALIFORNIA

Materials & Molecular Research Division

Submitted to Journal of the American Ceramic Society

CREEP AND DENSIFICATION DURING SINTERING OF GLASS POWDER COMPACTS: II. EFFECTS OF PARTICLE SIZE

M.N. Rahaman, L.C. De Jonghe, and R.J. Brook

December 1985

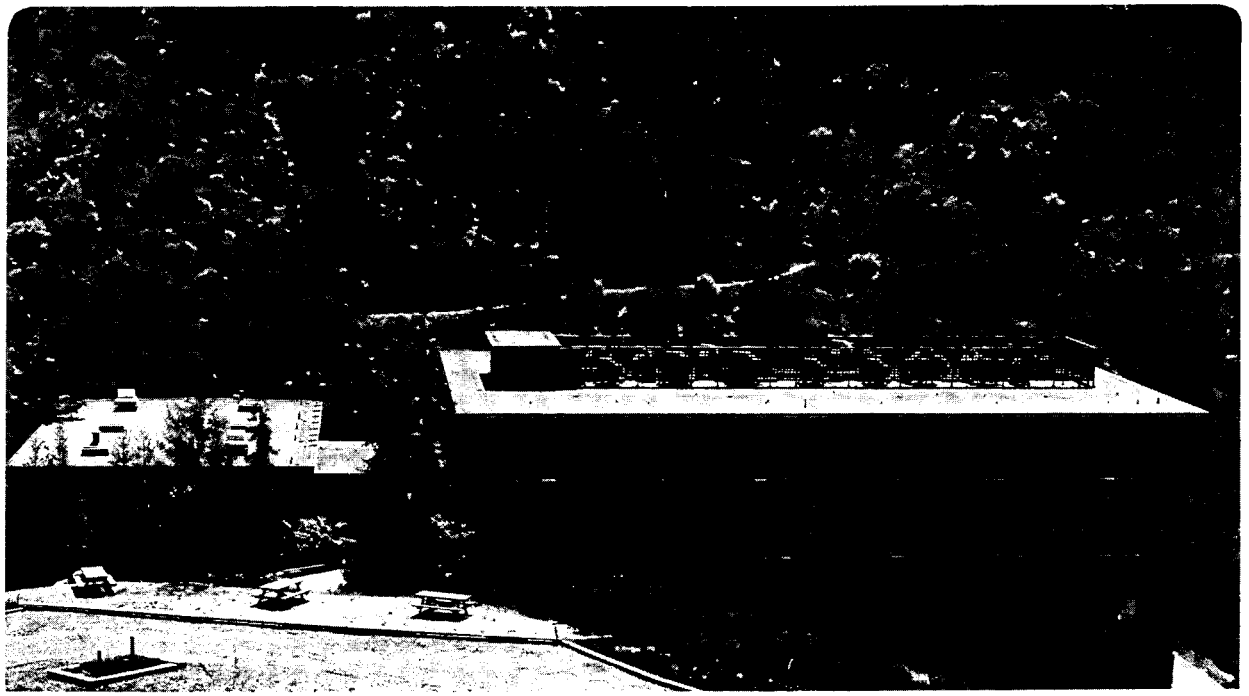

Prepared for the U.S. Department of Energy under Contract DE-AC03-76SF00098

DISCLAIMER

CREEP AND DENSIFICATION DURING SINTERING OF GLASS POWDER COMPACTS: II, EFFECT OF PARTICLE SIZE

M. N. Rahaman and L. C. De Jonghe
Materials and Molecular Research Division
Lawrence Berkeley Laboratory
and
University of California
Berkeley, CA 94720

R. J. Brook
Department of Ceramics
The University of Leeds
Leeds LS2 9JT
England

ABSTRACT

The simultaneous creep and densification behaviour of glass powder compacts was studied as a function of the particle size, G, at 605°C and for an applied stress of 9 kPa. The densification rate at any density is inversely proportional to G. A very important feature of the results is that the observed creep rate, $d\varepsilon/dt$, also shows a dependence on G. $d\varepsilon/dt$ increases as G decreases and may be expressed as the sum of two terms, i.e. $d\varepsilon/dt = \varepsilon_\rho^\circ/G + \sigma\varepsilon_\sigma^\circ$, where ε_ρ° and ε_σ° are constants for a particular powder system at fixed temperature, and σ is the applied stress. The term ε_ρ°/G represents a contribution to the observed creep rate from the densification process, and has the same 1/G dependence as the sintering stress (or the densification rate). These results provide further confirmation of the extensive interaction between the creep and densification processes in glass. Processes that may give rise to such an interaction are proposed.

Supported by the Division of Materials Science, Office of Basic Energy Sciences, U.S. Department of Energy, under Contract No. DE-AC03-76SF00098.

I. INTRODUCTION

A recent study[1] has indicated that there is significant interaction between creep and densification during the sintering of glass powder compacts. It was observed that the creep rate, $d\varepsilon/dt$, may be expressed as $d\varepsilon/dt = \dot{\rho}\dot{\varepsilon}^{\circ}_{\rho} + \sigma\dot{\varepsilon}^{\circ}_{\sigma}$, where $\dot{\varepsilon}^{\circ}_{\rho}$ and $\dot{\varepsilon}^{\circ}_{\sigma}$ are constants for a particular powder system at a fixed temperature. $\sigma\dot{\varepsilon}^{\circ}_{\sigma}$ represents a contribution from the applied stress, σ, increasing linearly with σ, while $\dot{\rho}\dot{\varepsilon}^{\circ}_{\rho}$, representing the contribution from the densification process, is proportional to the densification rate $\dot{\rho}$ (= $d\rho/dt$). The densification rate is defined by $d\rho/dt = \Sigma/\eta^{*}_{d}$, where Σ is the sintering stress, and η^{*}_{d} is the effective viscosity for the densification process. Since both Σ and η^{*}_{d} are functions of the density of the powder compact, the linear dependence of $d\varepsilon/dt$ on ρ cannot be used to determine its actual dependence on either Σ or η^{*}_{d}. In view of this complexity, the main objective of this paper is to explore the dependence of $d\varepsilon/dt$ on the particle size, G, of the glass powder. At a fixed density, Σ scales[2,3] as 1/G and η^{*}_{d} is expected to be constant.

Experimentally, simultaneous creep and densification experiments have been performed on polycrystalline oxides, [4-8] in which material transport occurs by diffusion processes. For such systems, the interaction between creep and densification is insignificant, suggesting that they are independent. These results clarify the secondary objective of this paper, which is the examination, at a qualitative level, of various mechanisms that would give rise to an interaction between creep and densification. Any mechanism will have

to account for the difference in magnitude of this interaction between glass and polycrystalline oxides.

There is, at present, no theory to account for the interaction between creep and densification. The models that consider combined creep and densification treat such processes as independent modes of deformation.[9,10]

II. EXPERIMENTAL PROCEDURE

A commercial soda-lime glass powder,* similar to the one used previously,[1] was first air-classified to obtain appropriate size fractions. After determining the average particle sizes using a scanning electron microscope, three fractions were selected and their particle sizes determined more accurately by counting the length intercepted by about 200 particles. Each powder fraction was uniaxially pressed at ~20 MPa into cylindrical compacts (6mm diameter by 6mm) with relative green densities of 0.55±0.01. About 10 vol % of Carbowax** was used as a binder.

Compacts were sintered in air for 2 to 3 hours in a loading dilatometer at 605°C and subjected to a constant applied load of 0.25N. The procedure for sintering the compacts in the loading dilatometer was described earlier.[1] The mass and dimensions of the compacts were measured before and after they were sintered and the final density was

*Owens-Illinois, Perrysburg, OH 43551

**Union Carbide Corporation, New York, NY 10017

measured using Archimedes' principle. In a separate set of experiments, sintering was terminated after times between 0 and 3h. The dimensions of these compacts were measured using a micrometer and the fracture surfaces were examined using a scanning electron microscope.

III. RESULTS

Fig. 1 shows micrographs of the three particle size fractions of glass powder used in the experiments. They are referred to by the letters A, B and C and their average particle sizes are 4μm (A), 8.5 μm (B) and 33μm (C). The spread in these values is about ± 10%. It is seen that the particles have angular shapes typical of crushed glass.

Friction between the push rods and the sample led to a small deviation from cylindrical geometry of the sample near its contact surfaces. This effect is insignificant, however, as outlined earlier.[1] Fig. 2 shows the results for the axial shrinkage, $\Delta L/L_0$ vs time, t, at 605 °C, at an applied load of 0.25 N for samples A, B and C (L_0 = initial sample length and $\Delta L = L - L_0$, where L = instantaneous sample length). The load of 0.25 N is equivalent to a stress of 9 kPa on the green compact and t = 0 represents the beginning of shrinkage. The load was applied quickly at t = 0 and the sintering temperature was reached after t = 8 min. Each curve is the average of two runs under the same conditions and each is reproducible to within ±2%. It is seen that, at any t, $\Delta L/L_0$ increases as the initial particle size, G, of the compact decreases.

Since the shrinkage of the compact is anisotropic, results for the radial shrinkage are also required during the course of the experiment in order to determine the creep strain and the volumetric strain. Fig. 3 shows the results for $\Delta L/L_o$ vs $\Delta D/D_o$ (D_o = initial sample diameter and $\Delta D = D-D_o$, where D = instantaneous sample diameter). The $\Delta L/L_o$ values are approximately proportional to $\Delta D/D_o$ and the slopes of the lines increase with decreasing particle size, i.e. the degree of anisotropic shrinkage is greater for larger particle sizes.

A methodology described by Raj[11] and the results of Figs. 2 and 3 were used to separate the creep strain from the volumetric strain due to densification. Fig. 4 shows the results for the relative density, ρ, vs time, t, for samples A, B and C. At any t, the values of ρ increase as G decreases. For the range of G used, there is a significant change in densification behaviour, e.g., for sample A, ρ reaches a value of ~ 0.95 after 2.5h, but for sample C, $\rho \sim 0.8$ after 3h.

The results for the creep strain, ε, vs time, t, are shown in Fig. 5 for samples A and C. The results for sample B has been omitted for reasons of clarity of this figure. At any t, the values of are not very different for samples A and C, but it should be remembered that the densities for these samples are quite different (at any t).

The relative densification rate, $d\rho/dt$, and the creep rate, $d\varepsilon/dt$, were obtained as a function of ρ (or t) by fitting smooth curves to the results of Figs. 4 and 5 and differentiating. As outlined earlier,[1] to evaluate $d\rho/dt$ and $d\varepsilon/dt$ vs ρ at a constant applied stress, σ, two

corrections have to be included: a compensation for the changing cross-sectional area of the sintering compact and for the the small change in the load applied by the spring of the linear voltage displacement transducer. Fig. 6 shows the results for $d\rho/dt$ and $d\varepsilon/dt$ vs ρ at σ = 9 kPa for samples A, B and C. It is seen that, at any ρ, both $d\rho/dt$ and $d\varepsilon/dt$ increase as the particle size, G, decreases. In addition, the curves for $d\rho/dt$ and $d\varepsilon/dt$ appear to have similar shapes.

Scanning electron micrographs of fracture surfaces of samples A and C sintered to ~0.78 and ~0.82, respectively, are shown in Fig. 7. Apart from a change in scale of the micrographs, the microstructures appear similar, i.e. the microstructures evolve in the same way, irrespective of the particle size of the compacts.

IV. DISCUSSION

As outlined earlier,[1] for a glass the creep rate, $\dot{\varepsilon}(\sigma)$ due to an applied stress, σ, and the relative densification rate, $d\rho/dt$, may be expressed by the following equations:

$$\dot{\varepsilon}(\sigma) = \sigma/\eta_c^* \qquad \text{Eqn. 1}$$

and

$$d\rho/dt = \Sigma/\eta_d^* \qquad \text{Eqn. 2}$$

where Σ is the sintering stress and η_c^* and η_d^* are the effective viscosities for creep and densification, respectively. For glass compacts having similar microstructures, at any ρ, both η_c^* and η_d^* are expected to be independent of particle size, G. Therefore, at constant ρ, the observed creep rate should be independent of G. This is clearly not observed experimentally as the results of Fig. 6 show. It appears

that a process with dependence on G is influencing and contributing to creep. An obvious process in these experiments is densification.

The sintering stress, Σ, is given by $\Sigma \sim \gamma/r$, where γ is the surface tension and r is the average pore radius. At any ρ, r is expected to increase with the scale of the system, i.e. with particle size, G. Accordingly, $d\rho/dt$ should be proportional to 1/G. Fig. 8 shows a plot of $d\rho/dt$ vs G_0/G for different values of ρ, where G_0 is a constant. It is seen that $d\rho/dt$ is indeed proportional to 1/G, except for small deviations in the data at $G_0/G \sim 1$, i.e. for sample C. These deviations arise because, for this sample, the hydrostatic component of the applied stress, $\sigma/3$, is not negligible compared to Σ. An estimate of the contribution to $d\rho/dt$ from σ can be made. From previous results (Ref 1, Fig. 10), it is estimated that for sample C, $\Sigma \sim 20$ kPa. The equivalent applied hydrostatic stress, i.e. $\sigma/3$ is 3 kPa. Lowering $d\rho/dt$ for sample C by a factor $\sigma/(\Sigma + \sigma/3)$, to remove the contribution from σ, makes the deviations insignificant.

Fig. 9 shows the results for the observed creep rate, $d\varepsilon/dt$, vs G_0/G for different values of ρ. It is seen that $d\varepsilon/dt$ increases linearly with 1/G and may be expressed by an equation of the form

$$d\varepsilon/dt = \dot{\varepsilon}^{\circ}_{\rho}/G + \dot{\varepsilon}(\sigma) \qquad \text{Eqn. 3}$$

where $\varepsilon(\sigma)$ is a linear function[1] of the applied stress, σ, and $\varepsilon^{\circ}_{\rho}$ is a function of the relative density, ρ. From Fig. 9, $\varepsilon(\sigma)$ was obtained at different ρ from the intercepts of the straight lines by using a simple least-squares fitting technique. The results for $\varepsilon(\sigma)$ vs

porosity, P, shown in Fig. 10 are almost identical to those obtained earlier (Reference 1, Fig. 9) by varying σ at constant G, and this provides further confirmation of the validity of Eqn 3. It is now clear that $\dot{\varepsilon}_\rho^\circ/G$ has exactly the same dependence on G as the sintering stress, Σ, (or the densification rate). We can therefore write

$$d\varepsilon/dt = \Sigma\dot{\varepsilon}_\rho^\circ + \sigma\dot{\varepsilon}_\sigma^\circ \qquad \text{Eqn. 4}$$

where $\dot{\varepsilon}_\rho^\circ$ and $\dot{\varepsilon}_\sigma^\circ$ are constants for a particular powder system at fixed temperature. $\Sigma\dot{\varepsilon}_\rho^\circ$ represents the contribution to the observed creep rate from the densification process, and $\sigma\dot{\varepsilon}_\sigma^\circ$ the contribution from the applied stress.

It is worth considering the types of mechanisms that would give rise to an interaction (or coupling) between creep and densification in glass. Such mechanisms should also be able to account for the observation that this interaction is insignificant in polycrystalline oxides. There are a number of important differences between glass and polycrystalline oxides (e.g. CdO), which are relevant to the creep-sintering behaviour of these two systems. First, there are no grain boundaries in sintered glass powder compacts. Second, the glass microstructure observed in this work has a very elongated pore morphology compared with the CdO system (see Ref. 1, Fig. 11). Third, the creep strains observed for glass are much larger than those observed in experiments on CdO.

The large creep strains observed in these creep-sintering experiments on glass can cause an extensive bias in the pore

morphology; this bias in turn leads to anisotropic densification.[12] In the methodology described by Raj[11] to separate the creep strain from the volumetric densification during creep-sintering, such anisotropic densification gives rise to a measureable creep contribution. Thus, for glass, in addition to constant volume creep driven by the applied stress, there may be a significant creep contribution due to shear induced anisotropic densification. In the CdO case, the more rounded pore morphology, in addition to the much smaller observed creep strains would predict that anisotropic densification is not a significant factor. At present it is not clear whether anisotropic densification can account fully fot the observed linear dependence of the creep rate on the densification rate.

Another mechanism which may give rise to extensive coupling between creep and densification is rearrangement. A small uniaxial (or shear) stress may be sufficient to trigger this type of "densifying rearrangement", although the overall driving force for the process is the sintering stress. The densifying rearrangement is constrained by the matrix and the must be compatible with the overall densification rate of the sample. Therefore, the rate of such a component of shear should be controlled by $d\rho/dt$. In addition, this type of rearrangement process would be expected to be severely limited in polycrystalline oxides after the initial stage of sintering.

The observed coupling mechanism between creep and densification during creep-sintering of glass powder compacts is, at present, poorly understood. The available experimental data do not permit a clear

distinction between the two processes, i.e. anisotropic densification and rearrangement, proposed to account for it. Additional creep-sintering experiments and microstructural measurements are in progress to resolve this problem.

ACKNOWLEDGMENT: The authors wish to thank R. M. Cannon for very helpful discussions.

REFERENCES

1. M. N. Rahaman and L. C. De Jonghe "Creep and Densification During Sintering of Glass Powder Compact: I, Effect of Applied Stress and Temperature". Previous article.

2. R. A. Gregg and F. N. Rhines, "Surface Tension and the Sintering Force in Copper, "Metall. Trans., 4 5 , 1365-74 (1973).

3. E. H. Aigeltinger, "Relating Microstructure and Sintering Force", Int. J. Powder Metall. Powder Tech., 11 3 , 195-203 (1975).

4. M. N. Rahaman and L. C. De Jonghe "Sintering of CdO Under Low Applied Stress", J. Am. Ceram. Soc., 67 10 , C-205-7 (1984).

5. M. N. Rahaman, L. C. De Jonghe and R. J. Brook "Effect of Shear Stress on Sintering", J. Am. Ceram. Soc., January, 1986.

6. M. N. Rahaman, L. C. De Jonghe and C. H. Hsueh, "Creep During Sintering of Porous Compacts", J. Am. Ceram. Soc. January, 1986.

7. M. N. Rahaman and L. C. De Jonghe, "Sintering of ZnO Under Low Applied Stress", Unpublished work.

8. M. Lin, M. N. Rahaman and L. C. De Jonghe, " Sintering and Creep of MgO Powder Compacts", for abstract see Am. Ceram. Soc. Bull. 64 (9) 219 (1985).

9. R. K. Bordia and R. Raj, "Sintering Behaviour of Ceramic Films Constrained by a Rigid Substrate", J. Am. Ceram. Soc. 68 6 , 287-92 (1985).

10. G. W. Scherer and T. Garino, "Viscous Sintering on a Rigid Substrate", J. Am. Ceram. Soc., 68 4 , 216-20 (1985).

11. R. Raj, "Separation of Cavitation-Strain and Creep-Strain During Deformation", J. Am. Ceram. Soc., 65 3 , C-46 (1982).

12. H. E. Exner, "Princiles of Single Phase Sintering", Rev. Powder Metall. Phys. Ceramics, 12 (1-4) 1-251 (1979).

LIST OF FIGURES

Fig. 1. Scanning electron micrographs of the three particle size fractions, A, B and C, used in the experiments. The average particle sizes are 4 μm (A), 8.5 μm (B) and 33 μm (C).

Fig. 2. Axial shrinkage vs time for samples A, B and C sintered at 605°C and subjected to 0.25N load.

Fig. 3. Axial shrinkage vs radial shrinkage for samples A, B and C.

Fig. 4. Relative density vs time for samples A, B and C.

Fig. 5. Creep strain vs time for samples A and C.

Fig. 6. Creep rate and relative densification rate vs relative density for samples A, B and C subjected to a constant uniaxial stress of 9 kPa and at 605°C.

Fig. 7. Scanning electron micrographs of fracture surfaces of (a) sample A at $\rho = 0.78$, and (b) sample C at $\rho = 0.82$.

Fig. 8. Relative densification rate vs inverse of the particle size for relative densities indicated.

Fig. 9. Creep rate vs inverse of the particle size for relative densities indicated.

Fig. 10. Creep rate component, due to an applied stress of 9 kPa, vs porosity.

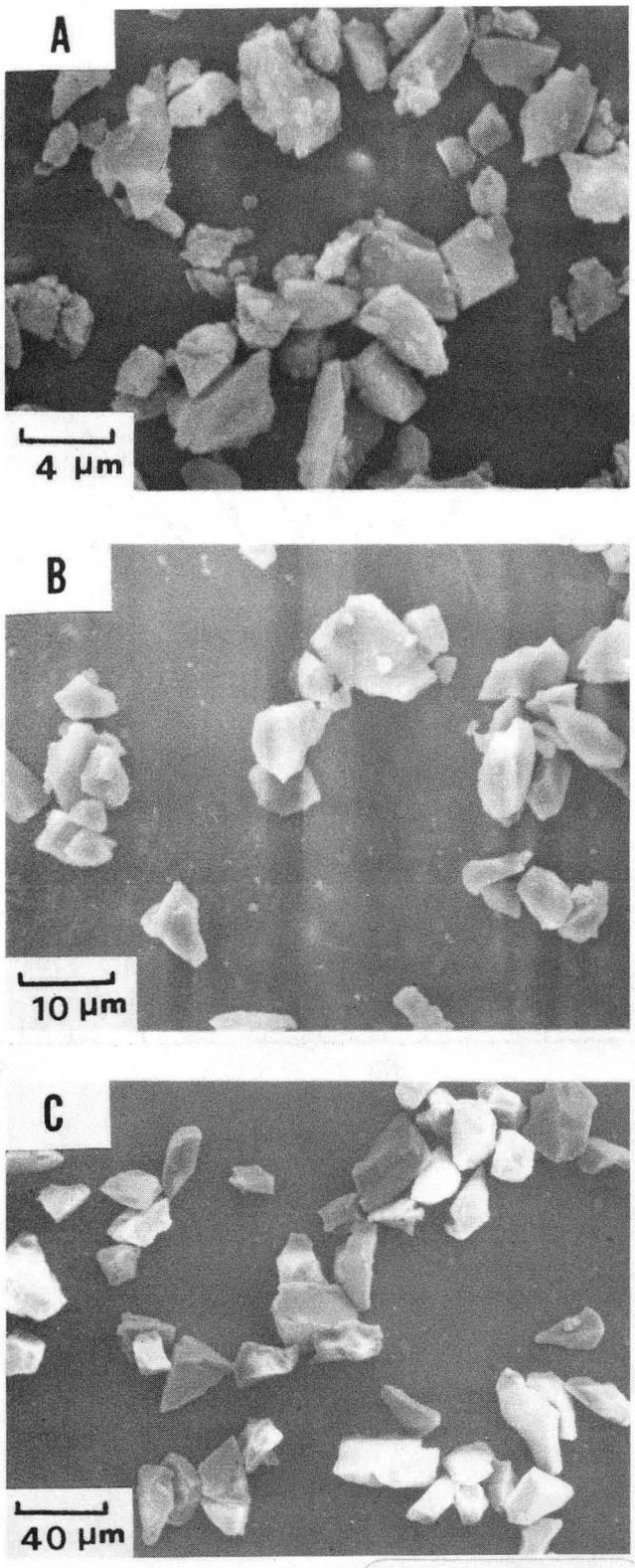

XBB 857-5481A

II: Fig. 1

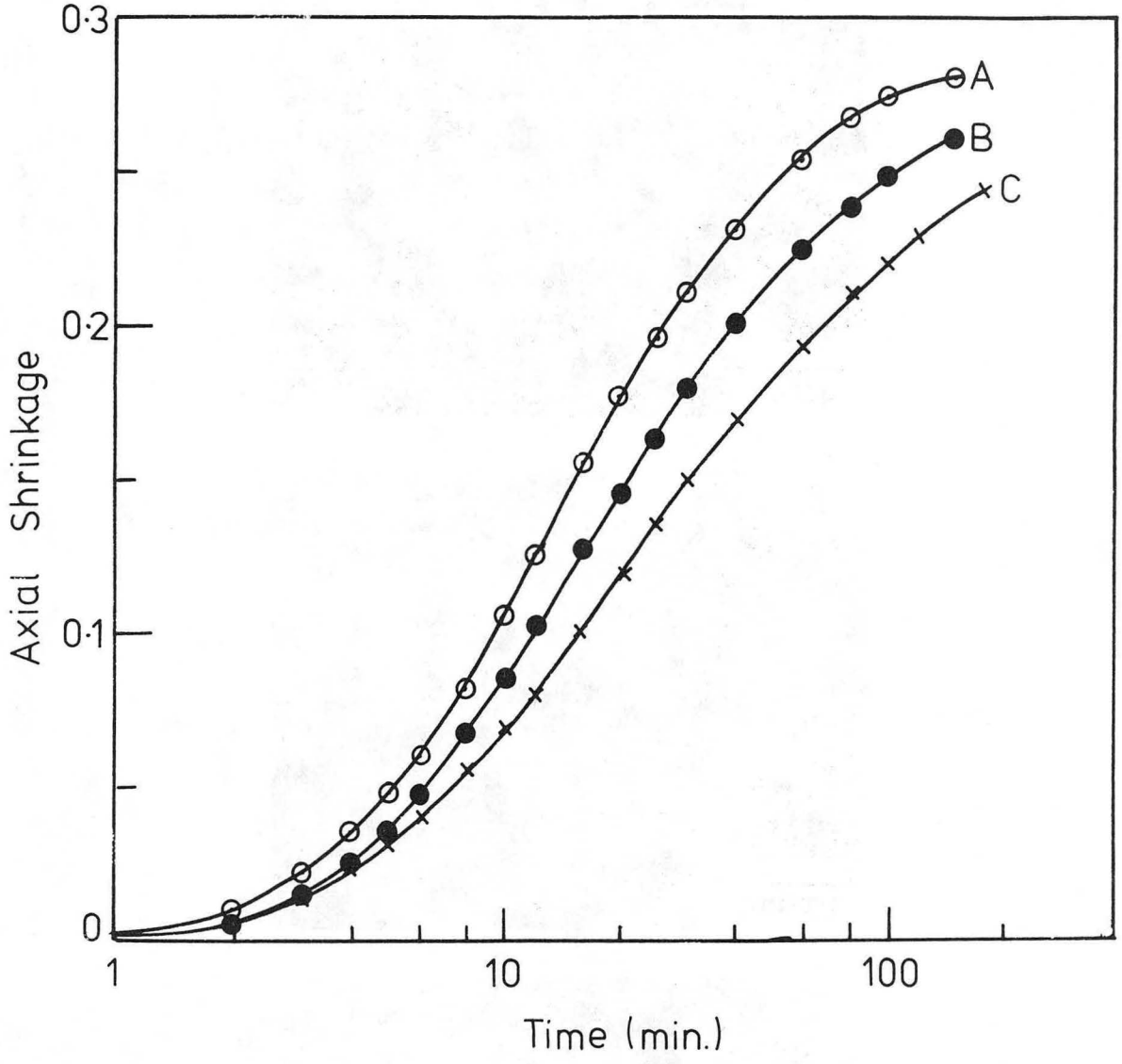

XBL 862-488

II: Fig. 2

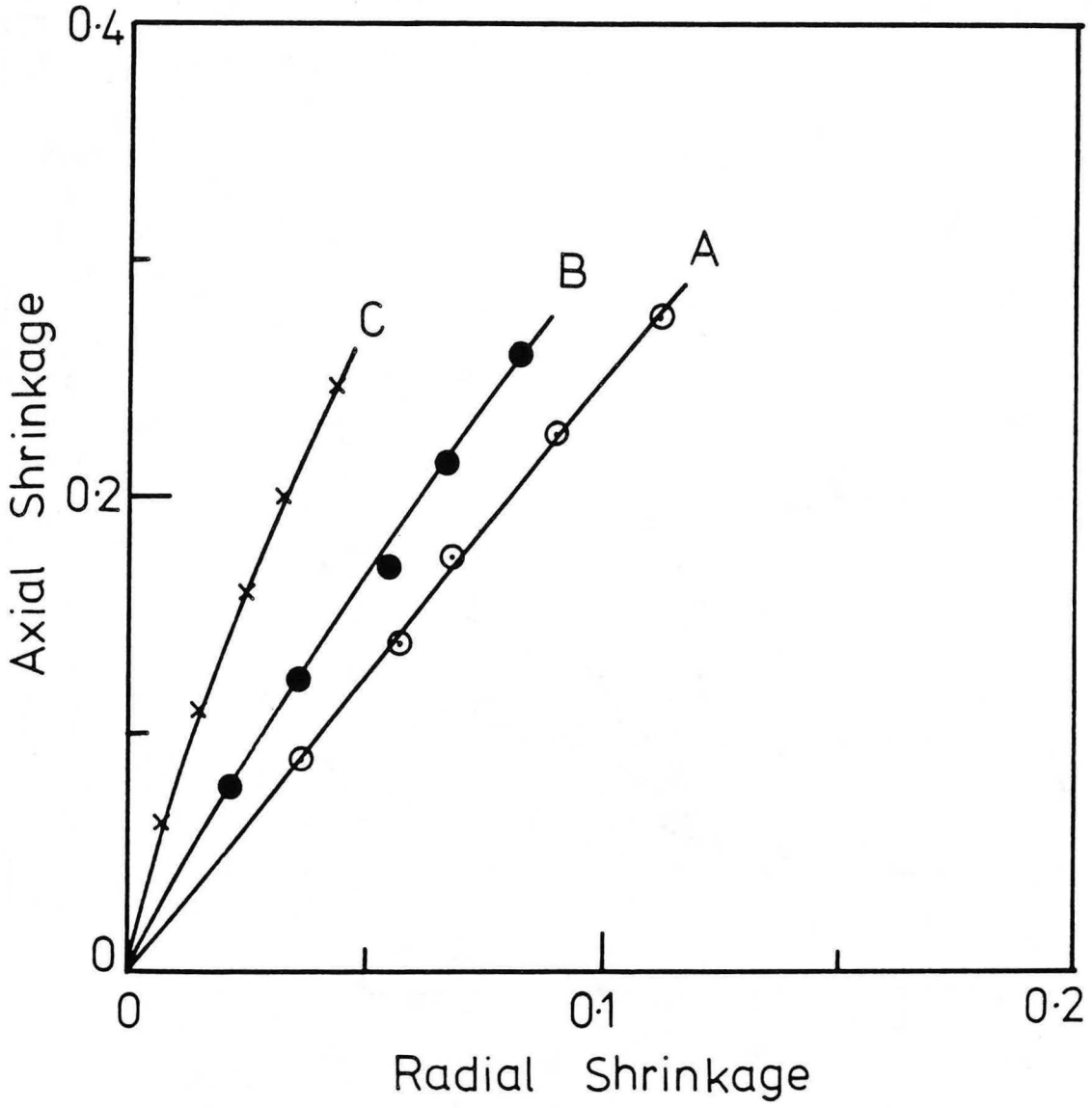

XBL 862-487

II: Fig. 3

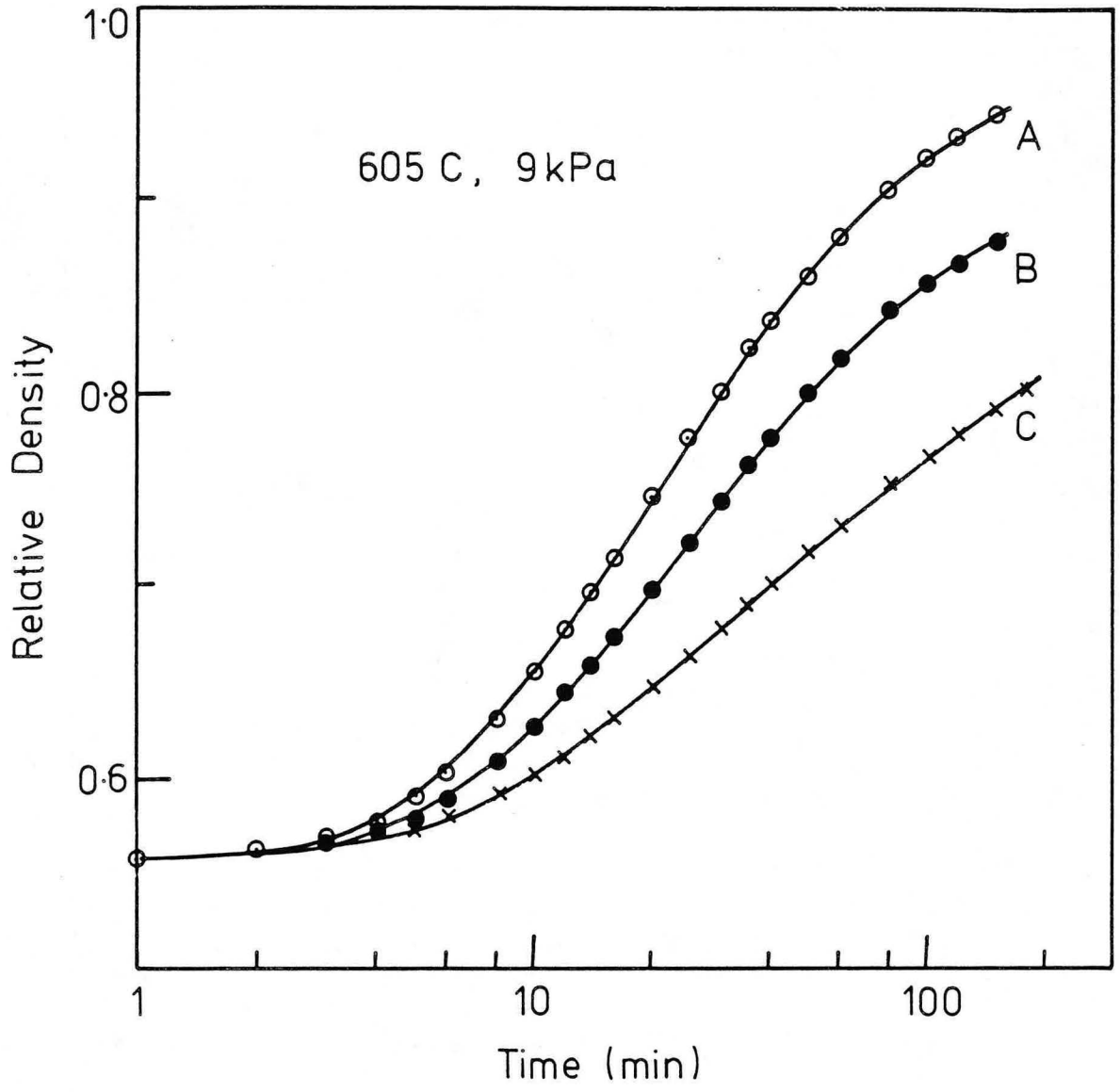

XBL 8510-4439

II: Fig. 4

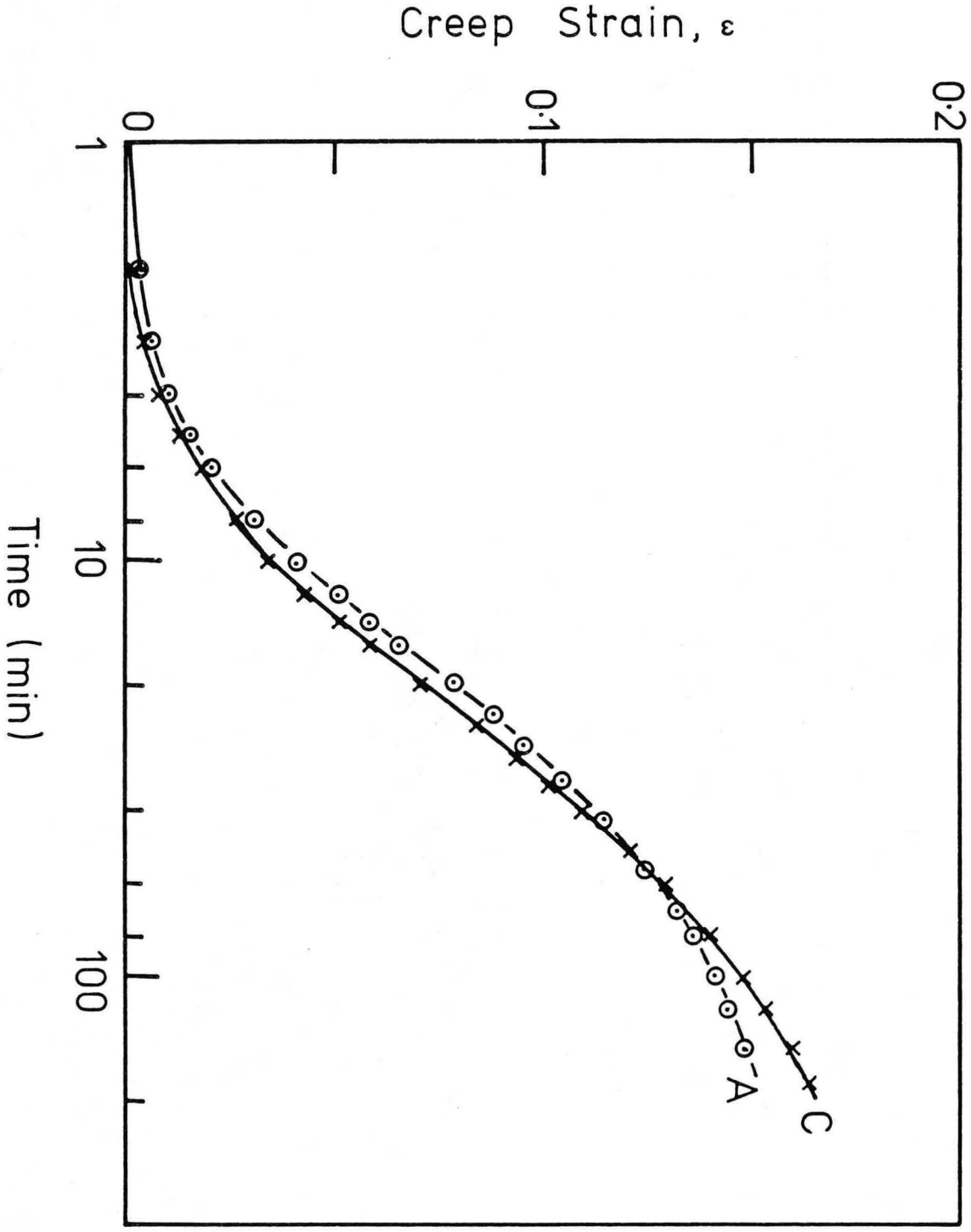

XBL 8510-4438

II: Fig. 5

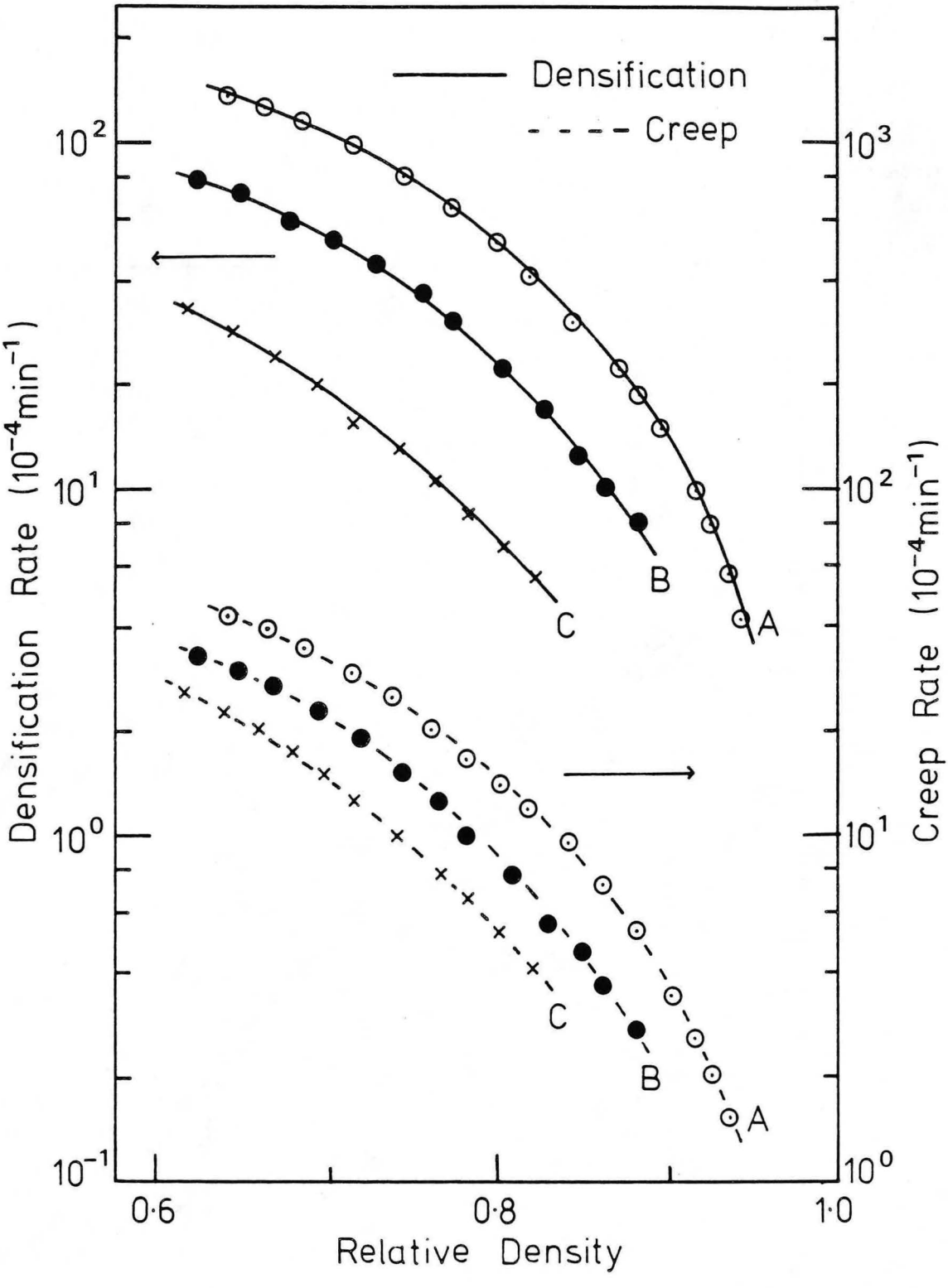

XBL 862-486

II: Fig. 6

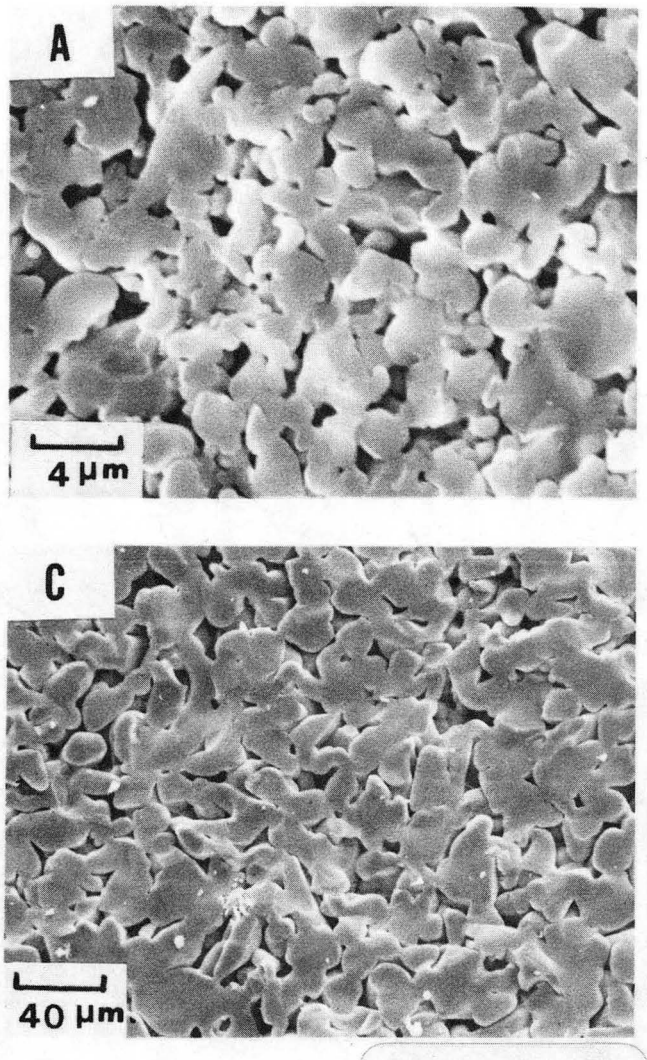

XBB 857-5476A

II: Fig. 7

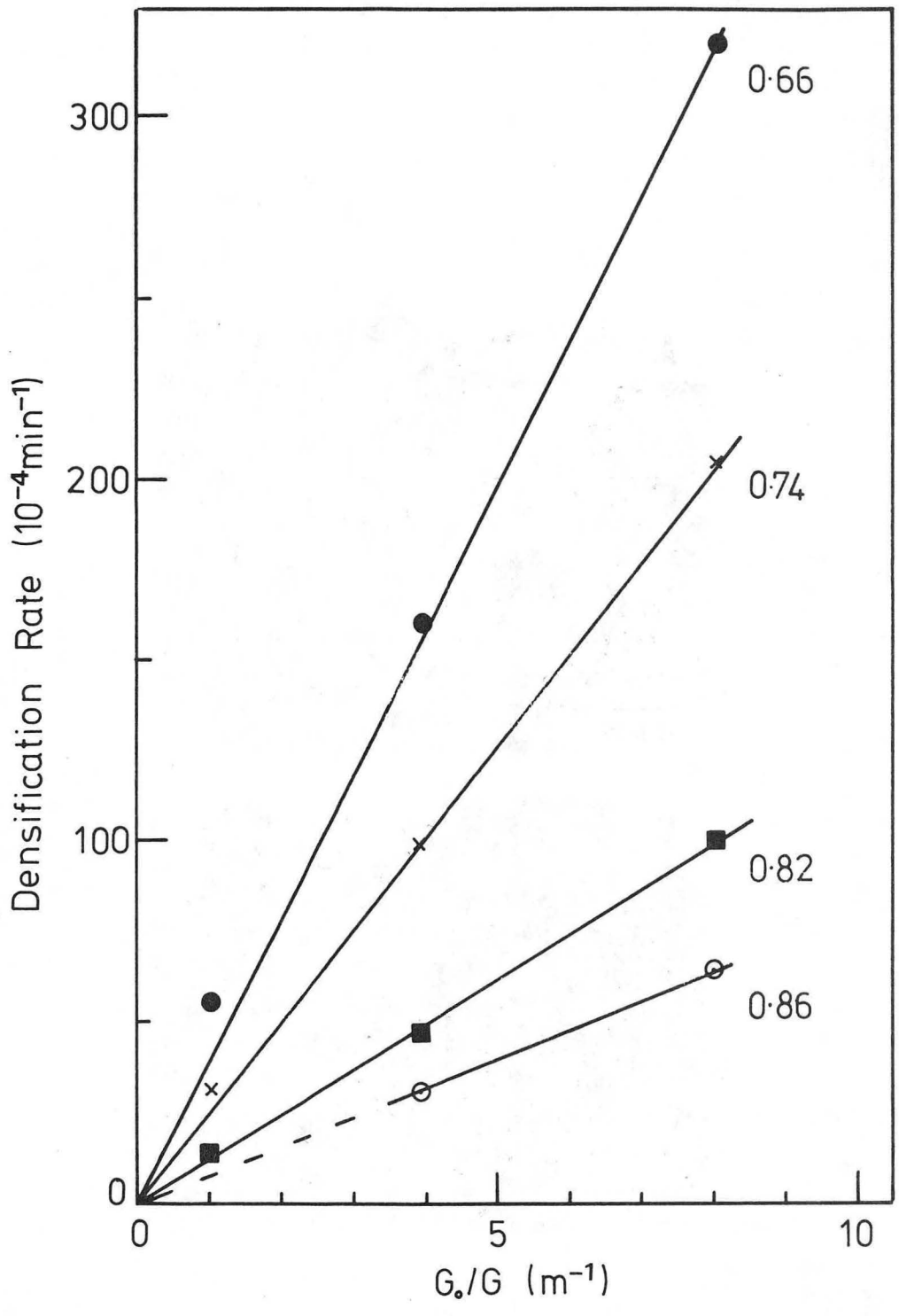

XBL 862-485

II: Fig. 8

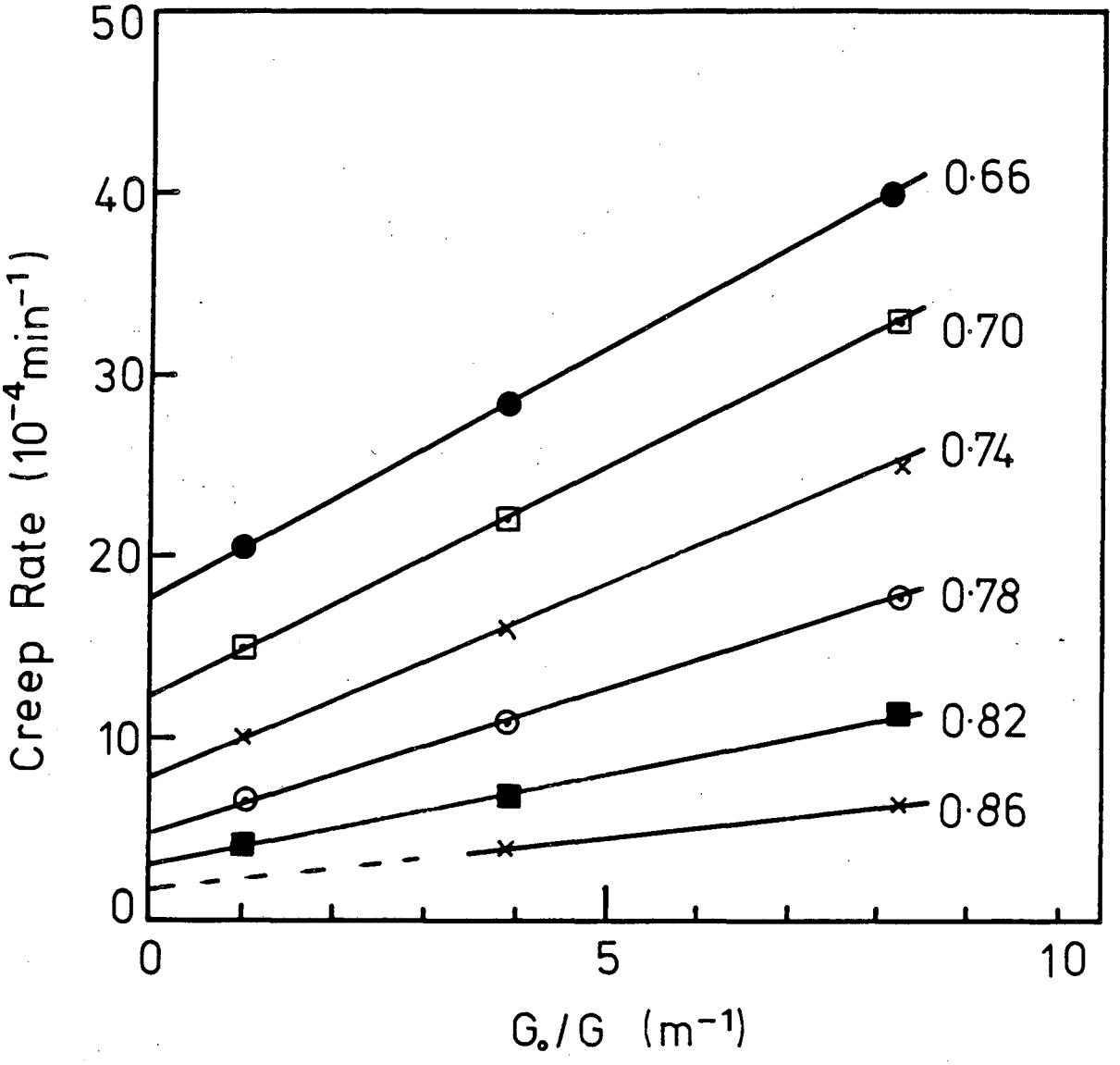

XBL 8510-4449

II: Fig. 9

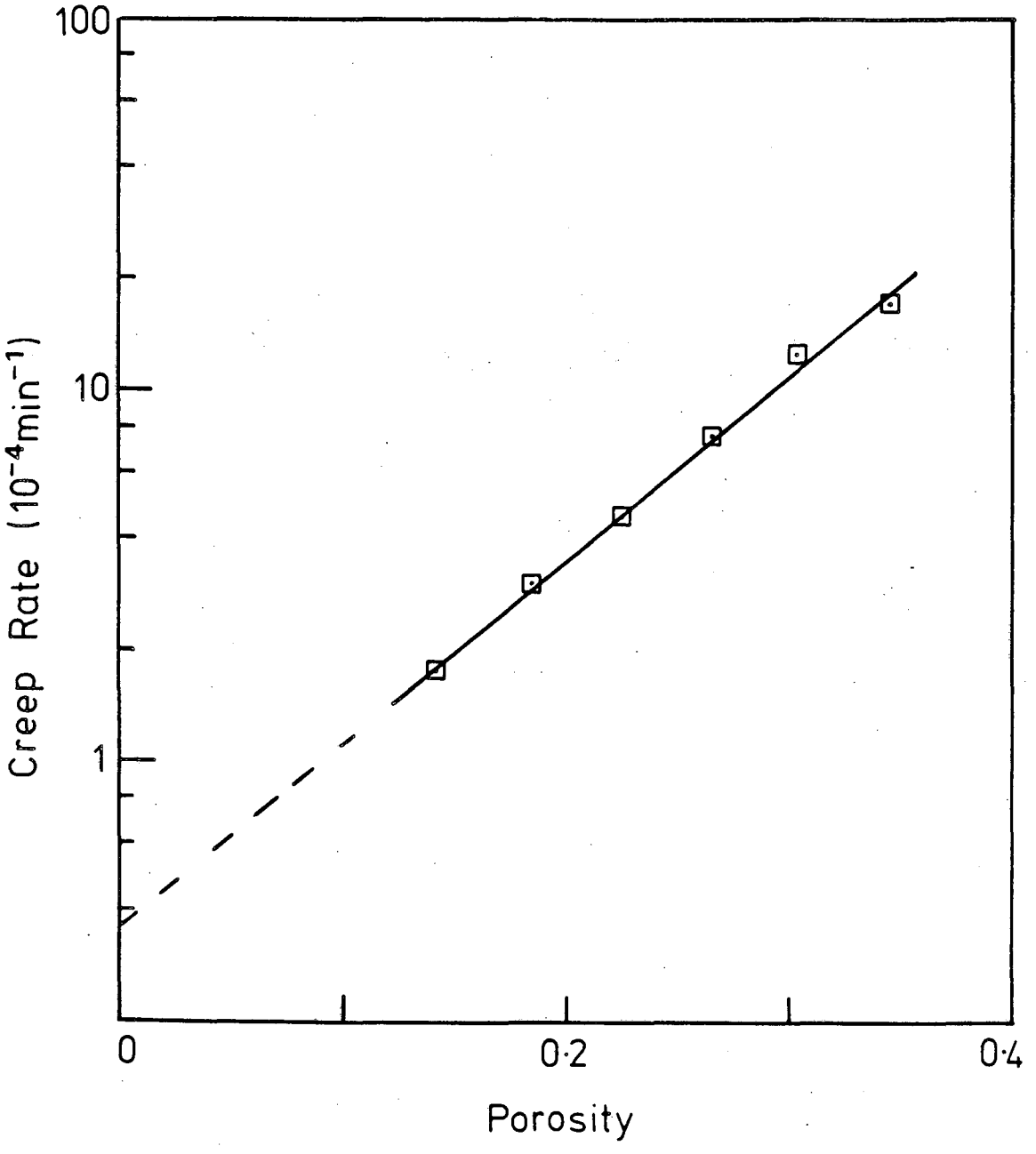

XBL 862-484

II: Fig. 10

LAWRENCE BERKELEY LABORATORY
TECHNICAL INFORMATION DEPARTMENT
UNIVERSITY OF CALIFORNIA
BERKELEY, CALIFORNIA 94720